Figure 7 | Manifold view of parameter degeneracy shared across solvers. (a)-(b) Principal-component projections of the fitted parameter vectors $\theta = \{R_s, L, R_{ct}, Q_1, \alpha_1, Q_2, \alpha_2\}$ onto low-dimensional subspaces (PC1–PC2 and PC1–PC3), comparing the continuous VQE/VQA solutions (points), discrete QAOA solutions (triangles), the classical baseline (×), and noisy refits at 2% complex noise (squares). The clustering and overlap illustrate that distinct optimization strategies converge to closely related regions in parameter space rather than isolated, solver-specific optima. (c) Explained variance of the leading principal components, highlighting that a small number of modes captures a substantial fraction of the variability in refit solutions, consistent with an underlying low-dimensional degeneracy structure. (d)-(e) Continuous-solver density contours (kernel density estimate) overlaid on the PCA scatter, showing the dominant "solution manifold" sampled by the continuous branch and demonstrating that the discrete QAOA candidates and noisy refits fall on the same manifold neighborhood anchored by the classical solution. Together, these projections provide geometric evidence that the apparent multi-solution behavior in MXene EIS fitting is governed by a shared correlated manifold rather than inconsistent solver behavior.

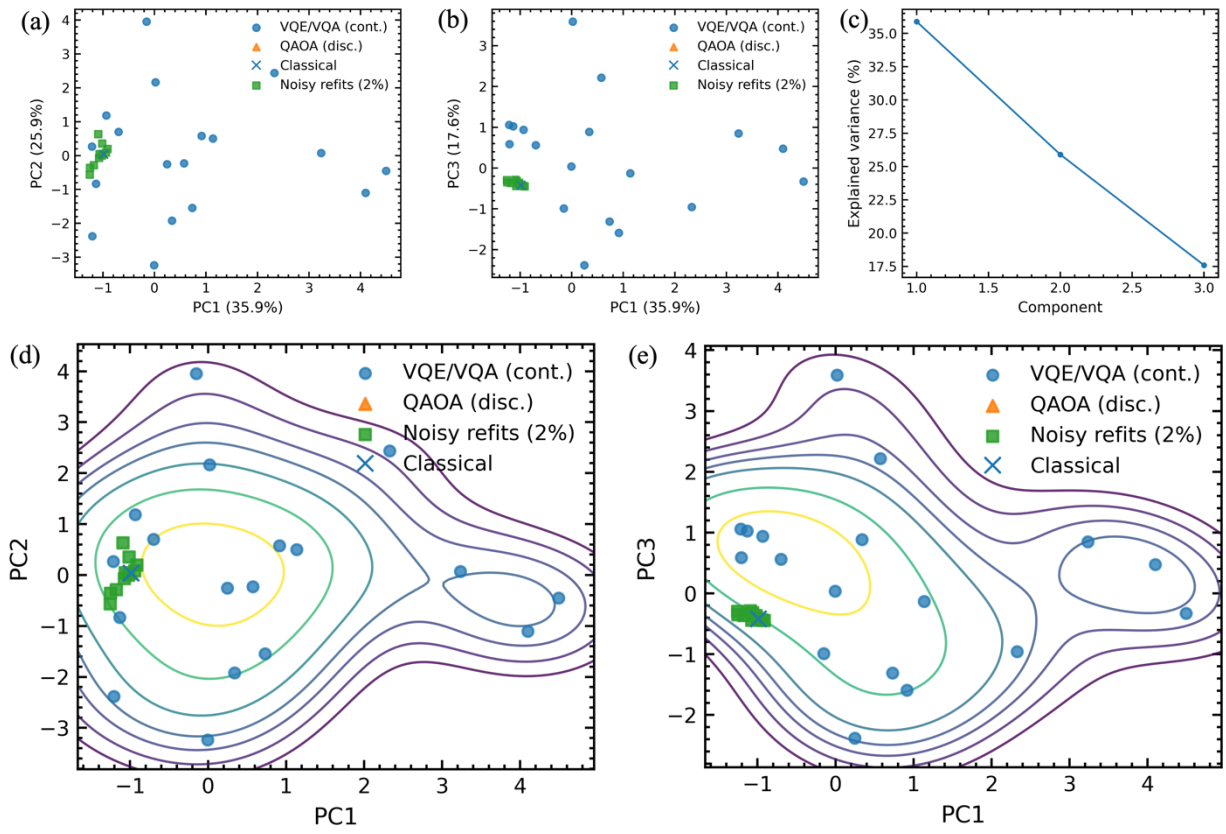
(a)
VQE/VQA (cont.)
QAOA (disc.)
Classical
Noisy refits (2%)
PC2 (25.9%)
PC1 (35.9%)
(b)
VQE/VQA (cont.)
QAOA (disc.)
Classical
Noisy refits (2%)
PC3 (17.6%)
PC1 (35.9%)
(c)
Explained variance (%)
Component
(d)
VQE/VQA (cont.)
QAOA (disc.)
Noisy refits (2%)
Classical
PC2
PC1
(e)
VQE/VQA (cont.)
QAOA (disc.)
Noisy refits (2%)
Classical
PC3
PC1